

ORIGINAL RESEARCH



## Profiling targetable immune checkpoints in osteosarcoma

Troy A McEachron<sup>a,b,c</sup>, Timothy J Triche<sup>b,d</sup>, Laurie Sorenson<sup>a</sup>, David M Parham<sup>d</sup>, and John D Carpten<sup>a,b</sup>

<sup>a</sup>Department of Translational Genomics; <sup>b</sup>Norris Comprehensive Cancer Center; <sup>c</sup>Department of Pediatrics, Keck School of Medicine of the University of Southern California, Los Angeles, CA, USA; <sup>d</sup>Department of Pathology, Children's Hospital Los Angeles, Los Angeles, CA, USA

### ABSTRACT

Osteosarcomas are aggressive bone tumors for which therapeutic advances have not improved over several decades. Unlike most pediatric tumors, the osteosarcoma genome is remarkably unstable, characterized by numerous copy number alterations and chromosomal structural aberrations. In this study, we asked if the targetable immune checkpoints *CD274 (PD-L1)*, *PDCD1LG2 (PD-L2)*, *CD276 (B7-H3)* and *IDO1* are impacted by copy number alterations in osteosarcoma. Of the 215 osteosarcoma samples investigated, *PD-L1/PD-L2*, *B7-H3* and *IDO1* were independently gained at frequencies of approximately 8–9%, with a cumulative frequency of approximately 24%. RNA sequencing data from two independent cohorts revealed that *B7-H3* is the most highly expressed immune checkpoint gene among the four investigated. We also show that *IDO1* is preferentially expressed in pediatric solid tumors and that increased protein expression of *B7-H3* and *IDO1* are significantly associated with inferior survival in patient samples. Using human osteosarcoma cell lines, we demonstrate that *IDO1* is gained in MG63 and G292 cells and that the *IDO1* inhibitor, epacadostat, inhibits the enzymatic activity of *IDO1* in a dose-dependent manner in these cells. Together, these data reveal the genomic and transcriptomic profiles of *PD-L1*, *PD-L2*, *B7-H3* and *IDO1* in osteosarcoma and identifies a potential context for targeted immunotherapeutic intervention in a subset of patients.

### ARTICLE HISTORY

Received 9 March 2018  
Revised 4 May 2018  
Accepted 7 May 2018

### KEYWORDS

Osteosarcoma; *PD-L1*; *PD-L2*; *B7-H3*; *CD276*; *IDO1*; checkpoint

## Introduction

Osteosarcoma is an aggressive bone tumor commonly observed in pediatric, adolescent, and young adult (AYA) patients. Unlike other solid tumors prominently seen in this age range, osteosarcomas exhibit a profoundly complex karyotype littered with chromosomal structural events, due, in part, to chromothripsis.<sup>1–4</sup> In the age of precision medicine, true molecularly targeted therapeutic options do not exist for patients with osteosarcoma. As a result, patients with osteosarcoma are treated using highly toxic chemotherapy regimens that have not changed in over 30 years.<sup>5,6</sup> Likewise, survival rates for patients with osteosarcoma have also remained stagnant over the last three decades with overall 5-year survival at roughly 65%.<sup>5</sup> For patients with metastatic disease, this rate drops to approximately 25%.

Recently, the field of immuno-oncology has gained incredible momentum in elucidating novel therapeutic approaches for patients suffering from a variety of malignancies, including immune checkpoint inhibitors, adoptive cell-based therapies, and numerous variations of bi-specific antibodies.<sup>7–16</sup> Several immune checkpoint inhibitors targeting the PD-1/PD-L1 axis and CTLA4 have demonstrated clinical efficacy in various malignancies and have thus gained FDA approval.<sup>17</sup> While the impact of these molecules in diseases such as melanoma, non-small cell lung cancer, and squamous cell head and neck cancer has been profound,



the same cannot be said for osteosarcoma or pediatric solid tumors as a whole.<sup>18–22</sup>

Recent reports suggest that increased somatic copy number alterations positively correlate with immune escape and poor response to immunotherapy.<sup>23</sup> Furthermore, increased aneuploidy is predictive of poor outcome in patients with osteosarcoma.<sup>4</sup> Together, these reports prompted our investigation to determine if the immune checkpoint genes encoding *PD-L1*, *PD-L2*, *B7-H3* and *IDO1* are amplified in osteosarcoma. We intentionally limited our investigation to include only tumor cell-derived immune checkpoint genes for which inhibitors are already FDA approved or are in late stage clinical development. Here, we describe the DNA copy number and gene expression profiles of *PD-L1*, *PD-L2*, *B7-H3*, and *IDO1* in osteosarcoma.


## Results

### Copy number gains of *PD-L1*, *PD-L2*, *B7-H3* and *IDO1* in osteosarcoma specimens

To investigate if the targetable immune checkpoint genes *PD-L1*, *PD-L2*, *B7-H3* and *IDO1* are affected by the copy number alterations that typify osteosarcoma, genome-wide copy number analysis was performed on DNA from 195 pediatric osteosarcoma tumor specimens using SNP 6.0 arrays. This copy number data was combined with whole genome

**CONTACT** Troy A. McEachron  [Troy.McEachron@med.usc.edu](mailto:Troy.McEachron@med.usc.edu)  Department of Translational Genomics, Keck School of Medicine of the University of Southern California, 1450 Biggy Street, Los Angeles, CA 90089-9601

Color versions of one or more of the figures in the article can be found online at [www.tandfonline.com/koni](http://www.tandfonline.com/koni).

 Supplemental data can be accessed [here](#)

© 2018 Taylor & Francis Group, LLC

sequencing data from the TARGET osteosarcoma project (19 specimens) and internal whole genome data (1 specimen), totaling 215 specimens. Our meta-analysis revealed recurrent independent copy number gains at genomic loci encompassing *PD-L1/PD-L2* (9p24.1), *B7-H3* (15q24) and *IDO1* (8p11.21) at frequencies of 8%-9% (Figure 1(a)). The nature of the *PD-L1*, *PD-L2*, and *IDO1* copy number alterations ranged from low-level gains to high-level amplifications (Figures 1(b-e) and 2(a-c)). Although *B7-H3* was gained in 8% of the specimens, we did not observe high level amplifications at this locus (Figures 1(d) and 2(b)). Furthermore, our data demonstrates a very strong correlation between samples with copy number gains of *PD-L1* and *PD-L2* (Figure 1(f)). With the exception of *PD-L1* and *PD-L2*, simultaneous gains of more than one checkpoint gene in an individual specimen were rarely observed, suggesting that these are mutually exclusive and independent events (Figure 1(a)).

### Gene expression of *PD-L1*, *PD-L2*, *B7-H3*, and *IDO1* in osteosarcoma and other pediatric malignancies

Using two different publically available RNA-sequencing datasets from the TARGET osteosarcoma project and the St. Jude Children's Research Hospital PeCan Data Portal, we compared the gene expression levels of *PD-L1*, *PD-L2*, *B7-H3* and *IDO1* in osteosarcoma specimens (TARGET,  $n = 81$ ; St. Jude,  $n = 23$ ). This analysis revealed that, in both datasets, *B7-H3* is robustly expressed while the expression of *PD-L1*, *PD-L2*, and *IDO1* are more modest (Figure 3; Table 1). We next sought to determine if the expression of these checkpoint genes varies between metastatic and non-metastatic osteosarcoma tissues. We did not observe statistically significant differences in the expression of *PD-L1*, *PD-L2*, or *B7-H3* in metastatic versus diagnostic samples in either the St. Jude or TARGET RNA sequencing datasets

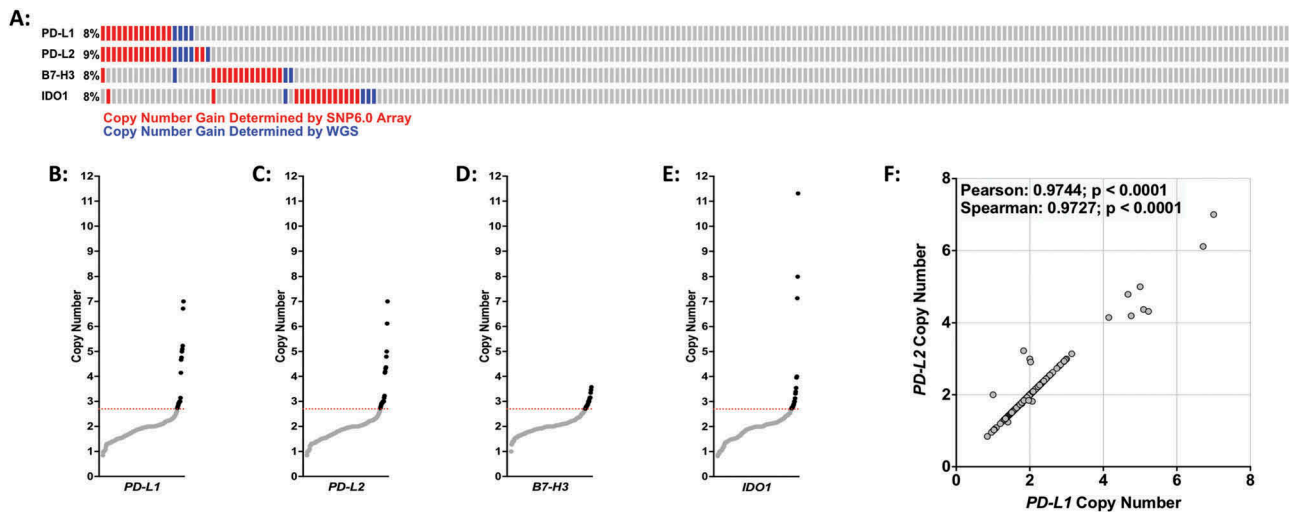


**Figure 1.** Copy number gains of *PD-L1*, *PD-L2*, *B7-H3*, and *IDO1* in osteosarcoma specimens. (A) Graphical depiction of *PD-L1*, *PD-L2*, *B7-H3*, and *IDO1* copy number gains in 215 osteosarcoma specimens. Red bars = copy number detected by SNP6.0 arrays; blue bars = copy number determined by whole genome sequencing. (B-E) DNA copy number distribution of (B) *PD-L1*, (C) *PD-L2*, (D) *B7-H3*, and (E) *IDO1* in osteosarcoma specimens where black dots indicate individual specimens with copy number values above threshold (2.7 copies; dotted red line). (F) DNA copy number scatter plot for *PD-L1* and *PD-L2*. Statistical significance ( $p \leq 0.05$ ) determined using both Spearman and Pearson correlation tests.

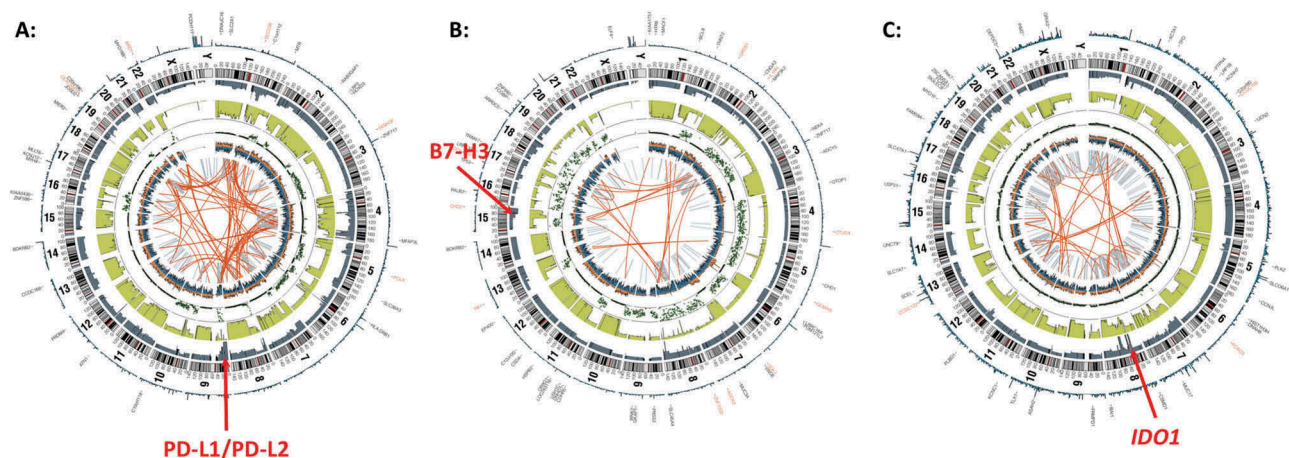


**Figure 2.** Copy number alterations at *PD-L1/PD-L2*, *B7-H3*, and *IDO1* loci revealed by whole genome sequencing. Representative circos plots of whole genome sequencing data from three individual patients indicating copy number gains at loci encoding (A) *PD-L1/PD-L2*, (B) *B7-H3*, and (C) *IDO1*. Red arrows point to locus of interest.

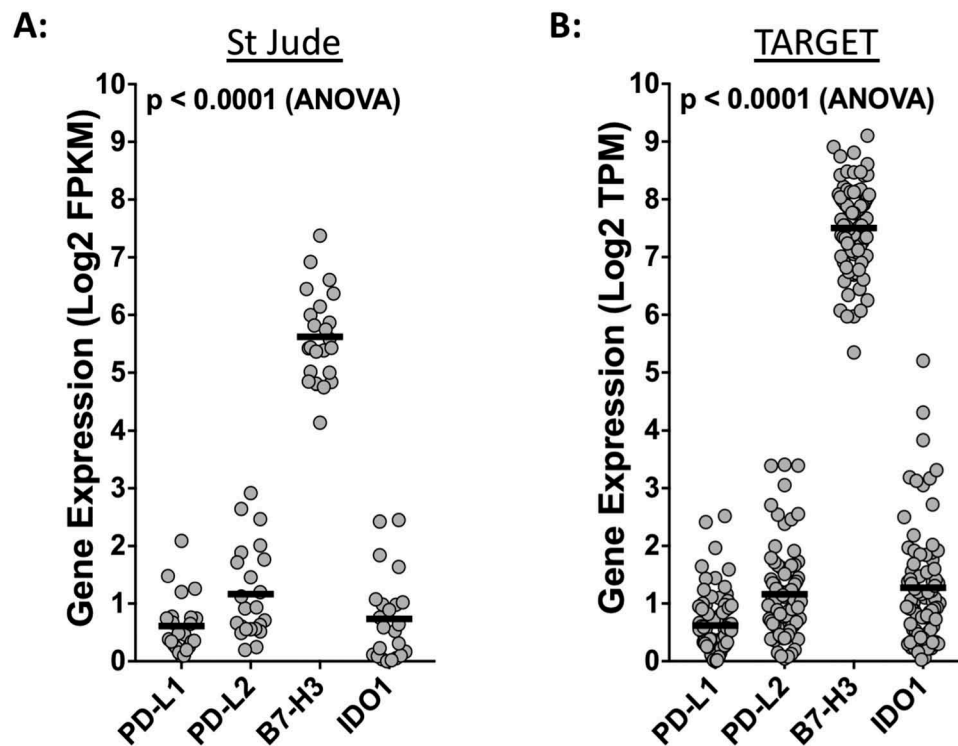


**Figure 3.** Osteosarcomas express high levels of *B7-H3*. Respective expression levels of *PD-L1*, *PD-L2*, *B7-H3*, and *IDO1* using RNA-sequencing data from the (A) St. Jude osteosarcoma and the (B) NCI TARGET osteosarcoma datasets. Statistical significance ( $p < 0.05$ ) was determined using ANOVA and corrected for multiple comparisons. P values for each comparison are listed in **Table 1**. FPKM, fragments per kilobase of transcript mapped; TPM, transcripts per million.

**Table 1.** P values from multiple comparison ANOVA.

Comparison	St. Jude P Value	TARGET P Value
<i>PD-L1</i> vs. <i>PD-L2</i>	<b>0.0214</b>	<b>&lt;0.0001</b>
<i>PD-L1</i> vs. <i>B7-H3</i>	<b>&lt;0.0001</b>	<b>&lt;0.0001</b>
<i>PD-L1</i> vs. <i>IDO1</i>	0.9083	<b>&lt;0.0001</b>
<i>PD-L2</i> vs. <i>B7-H3</i>	<b>&lt;0.0001</b>	<b>&lt;0.0001</b>
<i>PD-L2</i> vs. <i>IDO1</i>	0.1095	0.6955
<i>B7-H3</i> vs. <i>IDO1</i>	<b>&lt;0.0001</b>	<b>&lt;0.0001</b>

(Figures 4(a-c), (e-g)). While not quite statistically significant ( $p = 0.0507$ ), the St. Jude RNA sequencing data suggested that the mean expression *IDO1* is higher in metastatic osteosarcoma samples versus diagnostic samples (Figure 4(d)). This trend was not observed in the RNA sequencing data obtained from the larger TARGET osteosarcoma dataset (Figure 4(h)).

We then compared the expression levels of *PD-L1*, *PD-L2*, *B7-H3*, and *IDO1* in osteosarcoma to that of multiple pediatric hematologic, central nervous system (CNS), and non-CNS solid tumor types (Figure 5(a-d)). This analysis revealed that the mean expression of *PD-L1* in acute myeloid leukemia is significantly higher than that of osteosarcoma whereas the inverse is true for medulloblastoma (Figure 5(a)). Our data also demonstrates that, with few exceptions, the average expression of *PD-L2*, *B7-H3*, and *IDO1* is higher in osteosarcoma than in any of the tumor types analyzed (Figure 5(b-d)). Notably, we also observed that, as a group, non-CNS solid tumors expressed higher levels of *IDO1* when compared to either hematologic malignancies or CNS tumors (Figure 5(d)).

### Correlation analysis of immune checkpoint gene expression

We used the RNA sequencing dataset from the TARGET osteosarcoma project ( $n = 81$  specimens) to investigate the concordance in the expression of *PD-L1*, *PD-L2*, *B7-H3*, *IDO1*, and *CTLA4* (Figure 6). *CTLA4* was included in this analysis as this targetable immune checkpoint is expressed in infiltrating immune effector cells. While the expression of *B7-H3* did not correlate with the expression of any of the other immune checkpoints investigated, we did observe significant correlations in the expression of *PD-L1*, *PD-L2*, *IDO1*, and *CTLA4* (Figure 6). Of these data, the correlations between *IDO1* and *CTLA4* expression ( $r = 0.59$ ;  $p < 0.0001$ ) and between *PD-L1* and *PD-L2* expression ( $r = 0.64$ ;  $p < 0.0001$ ) were the strongest.

### Prognostic significance of *B7-H3* and *IDO1* protein expression in osteosarcoma tissues

Both descriptive and mechanistic studies have demonstrated that the PD-1/PD-L1 axis is associated with decreased survival in osteosarcoma.<sup>24–28</sup> As such, we decided to further investigate the prognostic value of *B7-H3* and *IDO1* expression. Immunohistochemical staining of an osteosarcoma tissue microarray (described in Table 2), representing 53% (*B7-H3*) and 55% (*IDO1*) of independent cases, revealed that increased expression of *B7-H3* significantly correlates with decreased survival (Figure 7(a)). *B7-H3* was consistently observed in tumor cells and in tumor associated blood-vessels

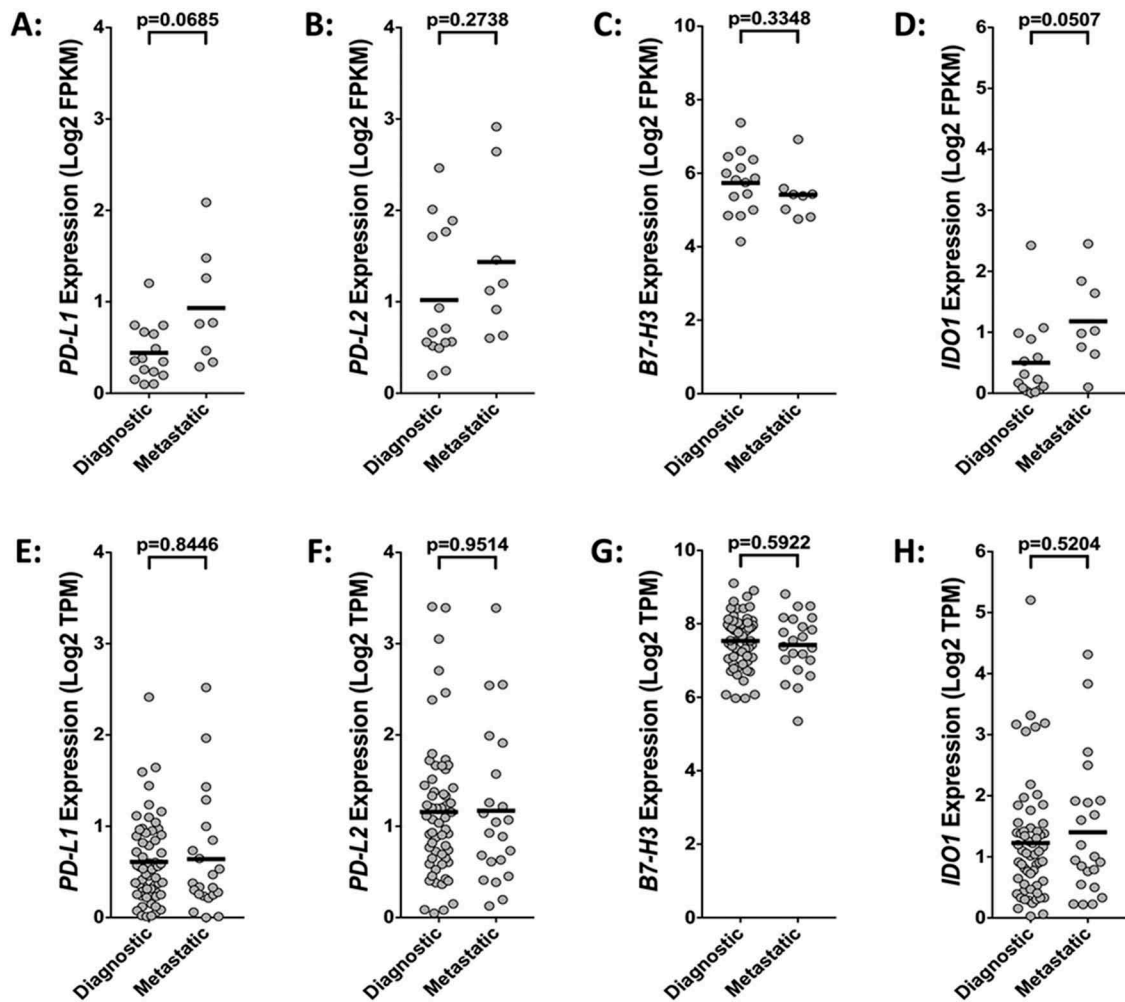


**Figure 4.** Disease status does not significantly influence the expression of immune checkpoint genes. Comparative analysis of (A, E) *PD-L1*, (B, F) *PD-L2*, (C, G) *B7-H3*, and (D, H) *IDO1* gene expression in diagnostic versus metastatic osteosarcoma samples using RNA-sequencing data from the (A-D) St. Jude osteosarcoma ( $n = 23$ ) and the (E-H) NCI TARGET osteosarcoma ( $n = 81$ ) datasets. Statistical significance ( $p \leq 0.05$ ) determined using unpaired two-tailed t-tests with Welch's correction. FPKM, fragments per kilobase of transcript mapped; TPM, transcripts per million.

(Figures 7(b-c), 8(a-b)). Likewise, immunohistochemical analysis of *IDO1* also revealed that increased expression significantly correlates with decreased survival (Figure 7(d)). *IDO1* staining was heterogeneous with variable immunoreactivity in both the tumor cells and subsets of non-malignant stromal cells, including the tumor-associated vasculature (Figures 7(e-f), 8(c-d)). Careful examination of a tissue core primarily composed of immune cells demonstrated variable *B7-H3* and *IDO1* positivity in different subsets of immune effector cells (Figure 8(b, d)). Consistent with the RNA sequencing data, we did not observe correlations between the expression of *B7-H3* and *IDO1* proteins (Supplemental Figure 1).

#### **Inhibition of *IDO1* activity in human osteosarcoma cell lines in vitro.**

Unlike *PD-L1*, *PD-L2*, *B7-H3*, and *CTLA4*, *IDO1* is an immunosuppressive enzyme with both autocrine and paracrine functions.<sup>29,30</sup> Because of these unique properties and its intriguing gene expression pattern (Figure 5(d)), we further

investigated *IDO1* *in vitro*. To validate the *IDO1* copy number data generated by the SNP6.0 arrays and whole genome sequencing, we performed copy number qPCR on genomic DNA from HOS, MG63, and G292 human osteosarcoma cell lines. HOS cells were diploid for *IDO1*, whereas both MG63 and G292 cells demonstrated *IDO1* copy number gains (Figure 9(a)). We also confirmed the protein expression of *IDO1* in the three osteosarcoma cell lines. Treatment with  $\text{IFN}\gamma$  for 24-hours resulted in the expression of *IDO1* in all three cell lines (Figure 9(b)). HOS cells exhibited minimal levels of *IDO1* and both MG63 and G292 cells demonstrated high level *IDO1* induction. The *IDO1* protein expression data from each cell line is consistent with the copy number qPCR data (Figure 9(a)).

Epacadostat is a selective inhibitor of *IDO1* enzymatic activity. We investigated the *in vitro* efficacy of epacadostat in MG63 and G292 cells by assaying the enzymatic activity of *IDO1* in the presence of increasing concentrations of the drug. While we were unable to reliably quantify kynurenine levels in the conditioned media from the cell lines by ELISA

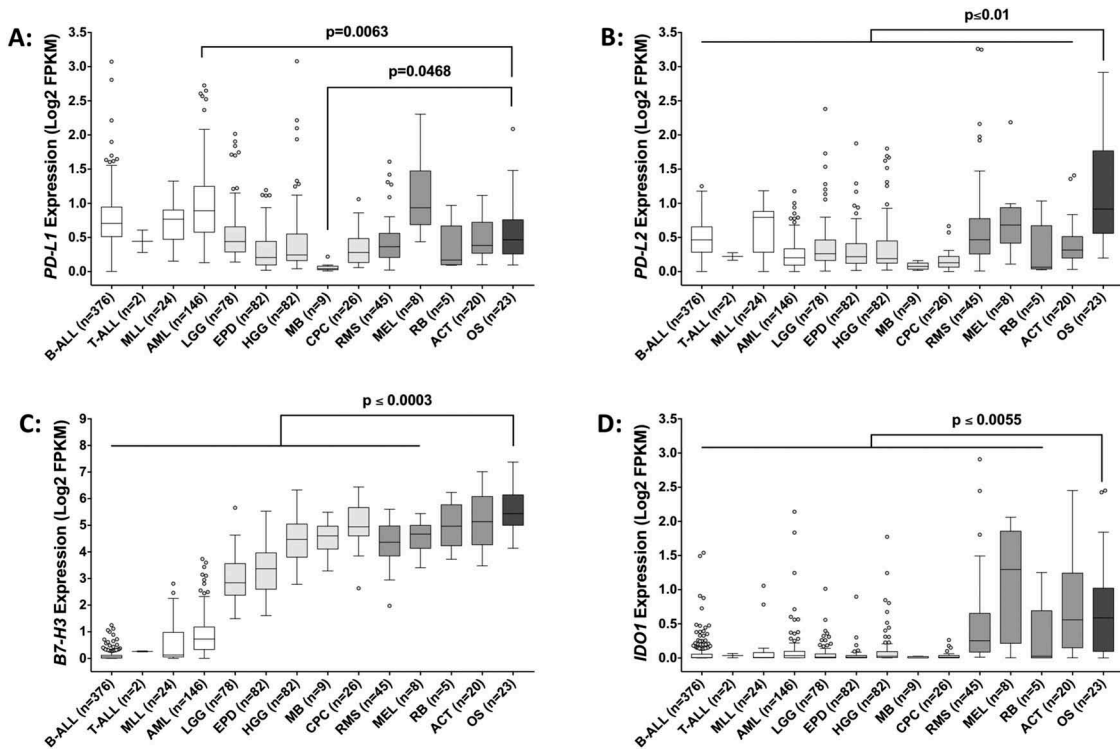


**Figure 5.** Expression of immune checkpoint genes across multiple pediatric tumor types. Gene expression of (A) *PD-L1*, (B) *PD-L2*, (C) *B7-H3*, and (D) *IDO1* across various pediatric hematologic malignancies (white bars), central nervous system tumors (light gray bars), solid tumors (gray bars), and osteosarcoma (dark gray bar). Statistical significance ( $p \leq 0.05$ ) was determined using one-way ANOVA with Holm-Sidak's multiple comparison test. P values are indicated for each pairwise comparison (vs. osteosarcoma). B-ALL, B-acute lymphoblastic leukemia; T-ALL, T-acute lymphoblastic leukemia; MLL, mixed lineage leukemia; AML, acute myeloid leukemia; LGG, low-grade glioma; EPD, ependymoma; HGG, high-grade glioma; MB, medulloblastoma; CPC, choroid plexus carcinoma; RMS, rhabdomyosarcoma; MEL, melanoma; RB, retinoblastoma; ACT, adrenocortical tumor; OS, osteosarcoma.

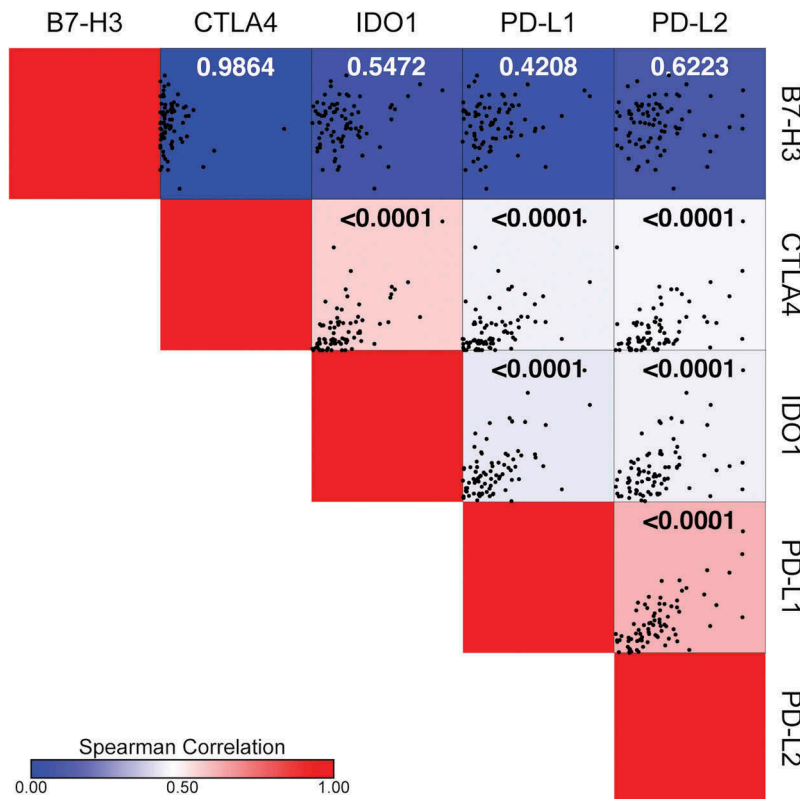


**Figure 6.** *B7-H3* expression does not correlate with the expression of *PD-L1*, *PD-L2*, *IDO1*, or *CTLA4*. Spearman correlation matrix illustrating gene expression correlations between *PD-L1*, *PD-L2*, *B7-H3*, *IDO1* and *CTLA4* using the TARGET osteosarcoma RNA sequencing dataset. Respective correlation X-Y scatter plots are shown within each square where each black dot represents an individual sample. Spearman correlation ( $r$ ) is indicated by the color bar where  $r$  values increase from blue ( $r = 0$ ) to red ( $r = 1$ ). Statistical significance ( $p \leq 0.05$ ) for each correlation is indicated in each square.

**Table 2.** Description of osteosarcoma TMA.

Age	Sex	Site	Diagnosis	IDO1 Analysis	B7-H3 Analysis
18	M	Femur	Osteosarcoma	Excluded	Excluded
44	F	Hip	Osteosarcoma	Excluded	Excluded
19	M	Femur	Osteosarcoma	Excluded	Excluded
44	F	Femur	Osteosarcoma	Excluded	Excluded
10	M	Femur	Osteosarcoma	Excluded	Excluded
10	M	Femur	Osteosarcoma	Excluded	Excluded
10	M	Femur	Osteosarcoma	Excluded	Excluded
10	M	Femur	Osteosarcoma	Excluded	Excluded
14	M	Femur	Osteosarcoma	Excluded	Excluded
14	M	Femur	Osteosarcoma	Excluded	Excluded
9	M	Femur	Osteosarcoma	Excluded	Excluded
12	F	Tibia	Osteosarcoma	Excluded	Excluded
9	F	Tibia	Osteosarcoma	Excluded	Excluded
11	M	Fibula	Osteosarcoma	Excluded	Excluded
18	M	Femur	Osteosarcoma	Excluded	Excluded
22	M	Humerus	Osteosarcoma	Excluded	Excluded
24	M	Popliteal Fossa	Synovial Sarcoma	Excluded	Excluded
23	M	Humerus	Osteosarcoma	Excluded	Excluded
27	M	Femur	Osteosarcoma	Excluded	Excluded
59	M	Mandible	Extraskeletal Osteosarcoma	Excluded	Excluded
29	M	Soft Tissue	Granulation Tissue	Excluded	Excluded
39	M	Femur	Osteosarcoma	Excluded	Excluded
61	F	Ilium	Radiation-Induced Sarcoma	Excluded	Excluded
11	M	Fibula	Osteosarcoma	Included	Excluded
11	M	Tibia	Osteosarcoma	Included	Excluded
26	M	Calcaneus	Osteosarcoma	Included	Excluded
11	M	Femur	Osteosarcoma	Excluded	Included
5	M	Femur	Osteosarcoma	Excluded	Included
24	M	Femur	Osteosarcoma	Included	Included
17	F	Femur	Osteosarcoma	Included	Included
16	M	Femur	Osteosarcoma	Included	Included
23	M	Bone	Osteosarcoma	Included	Included
14	F	Femur	Osteosarcoma	Included	Included
37	M	Pelvis	Osteosarcoma	Included	Included
17	M	Pelvis	Osteosarcoma	Included	Included
20	M	Femur	Osteosarcoma	Included	Included
20	M	Ilium	Osteosarcoma	Included	Included
17	M	Tibia	Osteosarcoma	Included	Included
20	M	Knee	Osteosarcoma	Included	Included
35	F	Humerus	Osteosarcoma	Included	Included
19	M	Femur	Osteosarcoma	Included	Included
16	M	Leg	Osteosarcoma	Included	Included
18	M	Femur	Osteosarcoma	Included	Included
11	F	Femur	Osteosarcoma	Included	Included
10	M	Femur	Osteosarcoma	Included	Included
18	M	Mandible	Osteosarcoma	Included	Included
13	M	Femur	Osteosarcoma	Included	Included
11	M	Tibia	Osteosarcoma	Included	Included
38	M	Mediastinum	Extraskeletal Osteosarcoma	Included	Included
34	F	Lung	Metastatic Osteosarcoma	Included	Included
24	F	Tibia/Fibula	Osteosarcoma	Included	Included
22	M	Humerus	Osteosarcoma	Included	Included
22	M	Tibia/Fibula	Osteosarcoma	Included	Included
20	F	Tibia	Osteosarcoma	Included	Included
17	F	Tibia	Osteosarcoma	Included	Included
16	F	Femur	Osteosarcoma	Included	Included
20	F	Femur	Osteosarcoma	Included	Included
31	F	Tibia	Osteosarcoma	Included	Included

(data not shown), we successfully measured tryptophan concentrations in the conditioned media of treated and untreated MG63 and G292 cell lines using a tryptophan repressor protein DNA binding assay. IDO1 activity and tryptophan concentration are inversely correlated. Epacadostat induced a dose-dependent increase in tryptophan levels, indicating a dose-dependent decrease in IDO1 enzymatic activity (Figure 9(c, e)). Consistent with its mechanism of action,

epacadostat did not alter the protein expression of IDO1 in the treated cell lines (Figure 9(d, f)).

## Discussion

Osteosarcomas are genomically unstable tumors exhibiting a high degree of aneuploidy and such aneuploidy has been implicated in immune escape.<sup>1-4,23</sup> Thus, we sought to determine if the targetable immune checkpoints *PD-L1*, *PD-L2*, *B7H3*, or *IDO1* are subject to copy number alterations in osteosarcoma. To our knowledge, this is the first report of somatic gains of immune checkpoints in osteosarcoma. Concordant copy number gains of both *PD-L1* and *PD-L2* was expected given that these two genes are within approximately 40kb of each other at the chromosome 9p24.1 locus. Moreover, this co-amplification has been observed in other malignancies including non-small cell lung cancer and triple negative breast cancer.<sup>31-33</sup>

In mining osteosarcoma RNA sequencing datasets from St. Jude Children's Research Hospital (n = 23) and the TARGET osteosarcoma project (n = 81) we observed a concordance in the gene expression patterns of *PD-L1*, *PD-L2*, *B7-H3*, and *IDO1* between the two studies, thus confirming the validity of each dataset. The relatively high expression of *B7-H3* in osteosarcoma was both striking and intriguing, as was the expression pattern of *B7-H3* across the various pediatric tumor types. According to the RNA expression overview in the Human Protein Atlas, *B7-H3* is expressed at low levels in the bone marrow, lymph nodes, and tonsils whereas additional studies report increased expression in a wide variety of non-hematological tumor types.<sup>34,35</sup> Together, these data suggest that the expression of *B7-H3* is restricted in lymphoid cells. This may explain the relatively low *B7-H3* expression observed in pediatric hematologic malignancies.

*B7-H3* protein expression has been reported in a variety of different cancers including non-small cell lung cancer, breast cancer, prostate cancer, renal cell carcinoma, high-grade gliomas, and giant cell tumor of the bone.<sup>34-36</sup> *B7-H3* also serves as a marker for tumor-associated endothelial cells.<sup>35,37</sup> Of particular relevance to osteosarcoma, *B7-H3* also has non-immunological functions in promoting osteoblast differentiation and bone development.<sup>38,39</sup> The relatively high level of expression of *B7-H3* in pediatric osteosarcoma and its role in normal bone development may circumvent the necessity for high-level gene amplifications.

*B7-H3* has been shown to exhibit both immunostimulatory and immunosuppressive effects and the exact mechanisms that underlie the immunosuppressive function of *B7-H3* are still under investigation.<sup>40-42</sup> Despite the seemingly contradictory roles of *B7-H3*, its potential as a therapeutic target is under active investigation. A recent report shows that blockade of *B7-H3* decreases tumor size and increases the number of CD8<sup>+</sup> tumor infiltrating lymphocytes in syngeneic models of pancreatic cancer and lung cancer.<sup>43</sup> Another report indicates that antibody-mediated inhibition of *B7-H3* reduces tumor growth as well as the number of tumor associated macrophages and myeloid derived suppressor cells in genetic

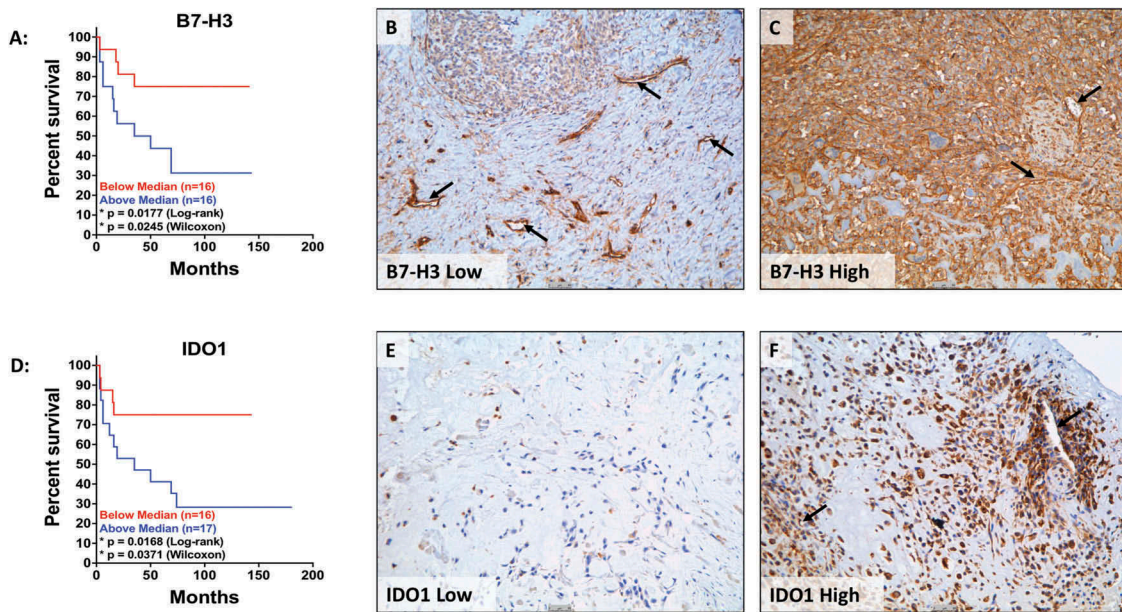


**Figure 7.** B7H3 and IDO1 protein expression independently correlate with decreased survival. Kaplan-Meier curves of (A) B7-H3 and (D) IDO1 expression in osteosarcoma TMA. Representative images of osteosarcoma tissue cores expressing (B) low levels of B7-H3, (C) high levels of B7-H3, (E) low levels of IDO1, and (F) high levels of IDO1. Low expression (red) is defined as IHC score below the mean and high expression (blue) is defined as IHC score above the mean. Statistical significance ( $p \leq 0.05$ ) was determined using both log-rank and Wilcoxon tests. Black arrows denote tumor vasculature. Scale bar = 50µm.

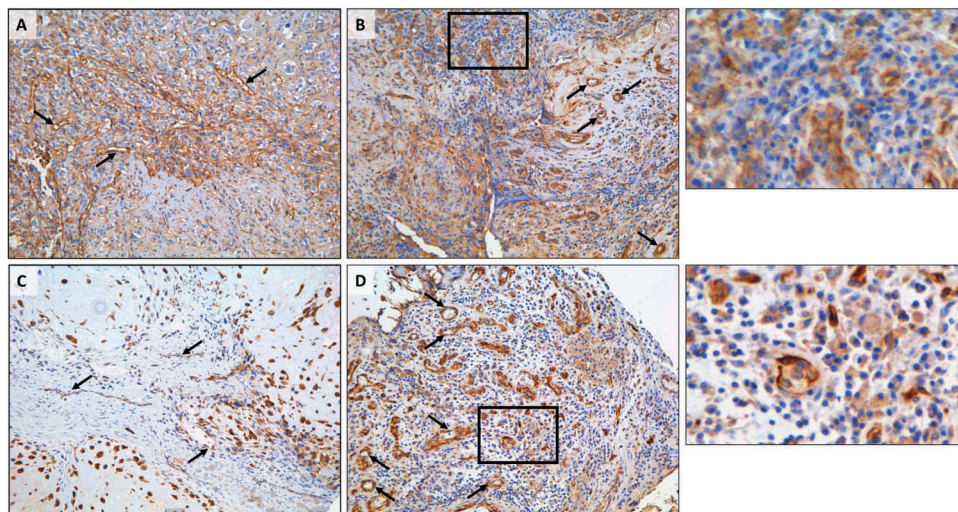


**Figure 8.** Heterogeneous expression of B7-H3 and IDO1 in osteosarcoma tissue. (A, C) Representative images of (A) B7-H3 and (C) IDO1 immunohistochemistry demonstrating immunoreactivity in malignant cells and tumor-associated vasculature. (B, D) Variable expression of (B) B7-H3 and (D) IDO1 in lymphoid aggregates. Black boxes indicate enlarged regions of interest (to the right of each panel). Black arrows denote tumor vasculature. Scale bar = 50µm.

models of head and neck squamous cell carcinoma.<sup>44</sup> The utility of B7-H3 as a therapeutic target is further supported by a recent report using xenograft and allograft models of various carcinomas to demonstrate the efficacy of B7-H3 antibody-drug conjugates (ADCs) to successfully target both tumor cells and tumor associated vasculature, prolong survival, and reduce metastasis.<sup>35</sup>

As it pertains to osteosarcoma, our data showing that increased B7-H3 expression correlates with poor survival is consistent with that of Wang *et al.*, collectively indicating that this molecule may be an attractive immunotherapeutic target in this disease.<sup>45</sup> Clinical approaches to selectively target B7-H3 include the use of enblituzumab (anti-B7-H3 antibody),

MGD009 (B7-H3 x CD3 DART), and the generation of CAR T-cells against B7-H3.<sup>46</sup> The expression and function of B7-H3 during normal bone development would argue against it being a therapeutic target for CAR T-cells.<sup>38,39</sup> However, it has been shown that antigen density rather than antigen expression dictates the anti-tumor efficacy of CAR T-cells.<sup>47</sup> Therefore, investigating the efficacy and specificity of B7-H3 CAR T-cell therapy in osteosarcoma is warranted.

*IDO1* expression is induced by inflammatory stimuli such as IFN $\gamma$ , interleukin-6 (IL-6), IL-12, and IL-18.<sup>48,49</sup> We hypothesize that this inflammatory microenvironment may underlie the increased *IDO1* expression observed in non-CNS solid tumors in comparison to both CNS and hematological malignancies.

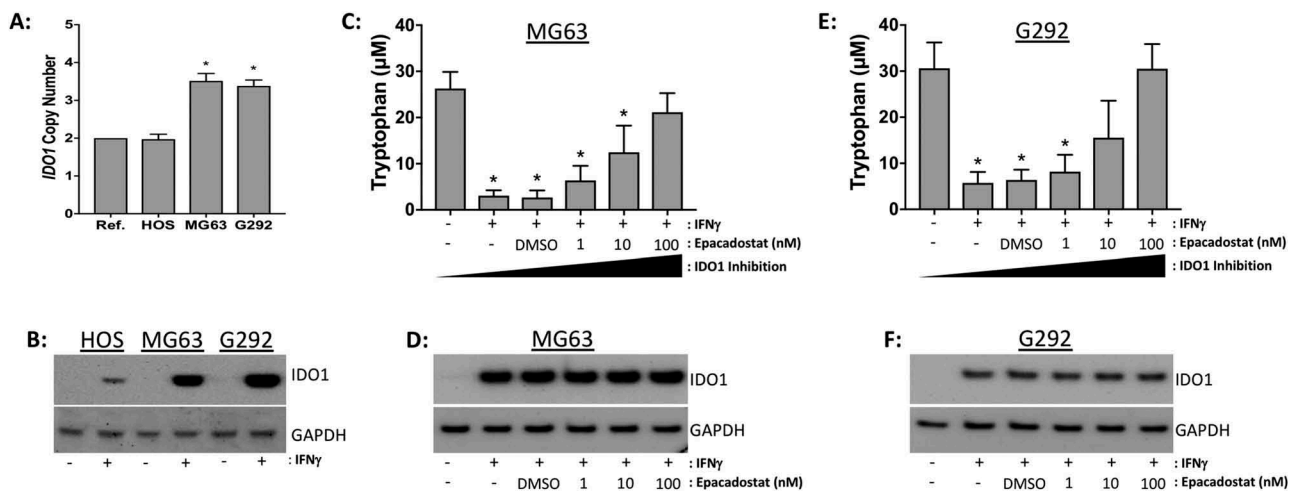


**Figure 9.** Epacadostat inhibits IDO1 function in G292 and MG63 human osteosarcoma cell lines *in vitro*. (A) DNA copy number profile of *IDO1* in HOS, MG63, and G292 cells. Ref, diploid reference DNA. (B) IDO1 western blot on whole cell lysates from osteosarcoma cell lines stimulated with serum free media (-) or IFN $\gamma$  (+) for 24-hours. GAPDH serves as the loading control. (C, E) Epacadostat decreases tryptophan metabolism in conditioned media from (C) MG63 and (E) G292 cell lines. Cells were pre-treated for 1-hour with the indicated doses of epacadostat then stimulated with serum free media (-) or IFN $\gamma$  (+) for 24-hours. Decreased tryptophan concentrations are indicative of increased IDO1 enzymatic activity. IDO1 protein expression in (D) MG63 and (F) G292 cell lines treated with epacadostat and IFN $\gamma$  as indicated below. Western blot images are representative of three independent experiments. Statistical significance ( $p \leq 0.05$ ) was determined using ANOVA and corrected for multiple comparisons (control vs. treated).

While we did not quantify IFN $\gamma$  expression in the available osteosarcoma samples, reports indicate that increased concentrations of circulating IFN $\gamma$  correlates with inferior outcome in patients with this disease.<sup>50</sup> This supports our finding and the work by Urakawa *et al.* indicating that IDO1 protein expression predicts poor outcome in osteosarcoma.<sup>51</sup> Taken together, these data suggest that the increased *IDO1* expression observed in osteosarcoma is a reflection of the inflammatory tumor microenvironment. Modulating the tumor microenvironment via targeted IDO1 inhibition is currently an active field of investigation with several drugs currently in various stages of clinical development, including epacadostat, indoximod, BMS-986,205, navoximod, and PF-06840003.<sup>29</sup> Since the initial submission of this manuscript, Bristol Myers-Squibb and Incyte Pharmaceuticals have halted phase 3 studies of their respective IDO1 inhibitors after the failure of epacadostat to meet its primary endpoint in melanoma.<sup>52,53</sup> Investigations into which patients are most likely to benefit from IDO1 inhibition will ensue as other early phase IDO1 trials are currently still active.<sup>52,53</sup> The data presented here identifies a subset of patients with osteosarcoma who may potentially benefit from targeted inhibition of IDO1 and highlights the utility of genome-informed approaches in immuno-oncology.

Consistent with our immunohistochemistry data, IDO1 expression and activity is not limited to tumor cells. Multiple cell types within the tumor microenvironment express IDO1, including tumor-associated fibroblasts, tumor-associated macrophages, and vascular endothelial cells.<sup>54-58</sup> Moreover, the resultant effect of IDO1 enzymatic activity traffics myeloid derived suppressor cells and regulatory T-cells into the tumor stroma.<sup>59,60</sup> Thus, while standard RNA sequencing is capable of detecting *IDO1* expression in a heterogeneous tissue sample, this approach is incapable of determining its cellular source. Such resolution would require single-cell RNA sequencing or multiplexed imaging.<sup>61,62</sup> Nevertheless, due to its paracrine effects, whether IDO1 is expressed in tumor cells, infiltrating host cells,

or both may not be nearly as important as its activity and ability to promote an immunosuppressive microenvironment.<sup>29,30,63</sup> Further investigation is needed to understand the autocrine effects of IDO1 in osteosarcoma and how gains of IDO1 impact the aryl-hydrocarbon signaling pathway.

To date, results from clinical studies investigating the use of immune checkpoint inhibitors in patients with bone sarcomas have been largely underwhelming.<sup>18-20,64,65</sup> In the Alliance A091401 trial, single agent PD-1 blockade using nivolumab failed to meet the primary endpoint of overall response in an unselected cohort of pre-treated sarcoma patients with advanced disease, including bone sarcomas.<sup>18</sup> Similar results were observed in the SARC028 trial where single agent pembrolizumab demonstrated activity in select soft tissue sarcomas but proved to be insufficient for patients with osteosarcoma.<sup>20</sup> The precise mechanism(s) by which single agent PD-1 blockade is rendered ineffective in osteosarcoma is not yet known. However, in a trial demonstrating limited efficacy of pembrolizumab in patients with advanced soft tissue sarcomas, increased kynurenine levels (indicative of IDO1 activity) was observed during treatment, suggesting that IDO1 may contribute to the failure of PD-1 inhibition in this specific context.<sup>66</sup> Moreover, Holmgaard *et al.* used the B16 murine melanoma model to show that genetic ablation of murine IDO1 increased the therapeutic efficacy of PD-1/PD-L1 inhibition.<sup>67</sup> This report also showed that inhibition of CTLA4 synergized with IDO1 inhibition in both melanoma and breast cancer models.<sup>67</sup> These data, combined with our findings that there are significant correlations between the expression of *PD-L1*, *PD-L2*, *IDO1*, and *CTLA4*, provides rationale that combination immunotherapy may provide a therapeutic benefit for patients suffering from osteosarcoma.

The data presented here represents the first report of the genomic and transcriptomic profiles of targetable immune checkpoints in osteosarcoma. A comprehensive and integrated genomic, transcriptomic, and proteomic profiling in



a larger cohort of clinically annotated osteosarcoma samples will need to be performed to elucidate the full spectrum of immune checkpoints and molecularly dissect the osteosarcoma microenvironment. Our data indicates that there is marked heterogeneity in the expression of immune checkpoints in osteosarcoma. As demonstrated by Dix Junqueira Pinto *et al.* the information obtained from any given core on a TMA may not be representative of the entire tissue section.<sup>68</sup> Therefore, the use of whole tumor sections versus TMAs will be essential to faithfully examine the expression of immune checkpoints and assess the tumor microenvironment in heterogeneous solid tumor specimens. In addition, *in vivo* studies using immunocompetent osteosarcoma models will help clarify the functional significance of *PD-L1*, *PD-L2*, *B7-H3*, and/or *IDO1* copy number gains as they pertain to the osteosarcoma microenvironment and immune evasion mechanisms.

## Materials and methods

### Cell culture

HOS and MG63 cell lines were a gift from Dr. Alan Epstein (USC). G292 cells were obtained from ATCC (CRL-1423). Cell lines were grown in RPMI1640 (Invitrogen) supplemented with GlutaMax (Invitrogen) and 10% fetal bovine serum (Omega Scientific). Cells were checked for mycoplasma (Lonza) and their identities confirmed with short tandem repeat profiling (Cell Line Genetics). Recombinant IFN $\gamma$  was purchased from R&D Systems. Prior to treatment, cells were grown to near-confluence and serum starved for 6-hours in RPMI1640. One hour prior to IFN $\gamma$  stimulation, cells were treated with epacadostat (Selleck Chemicals) or dimethyl sulfoxide (Sigma). IFN $\gamma$  was added to the respective wells at a final concentration of 50ng/mL. Cell lysates and conditioned media were harvested 24-hours post-treatment.

### DNA copy number assays

Copy number data was obtained using the Affymetrix Genome-Wide Human SNP Array 6.0 platform. The array data was analyzed with Partek Genomics Suite (Partek). Raw .CEL files were normalized for probe length and GC content. Diploid copy number baseline files for the SNP6.0 arrays were generated using 794 HapMap samples and subsequently used for comparative copy number analysis. Copy number values greater than 2.7 were interpreted as a copy number gain. Matched tumor-normal whole genome sequencing data from 19 pediatric osteosarcoma specimens was obtained from the TARGET Osteosarcoma database (<https://ocg.cancer.gov/programs/target/projects/osteosarcoma>). TaqMan copy number assays for CD276/B7H3 (assay ID: Hs05355907\_cn), IDO1 (assay ID: Hs00636720\_cn), and the TaqMan copy number RNaseP reference assay (cat #: 4403326) were purchased from ThermoFisher and performed according to the manufacturers protocol. Pooled human genomic DNA (Promega) was used as the diploid reference DNA for the TaqMan copy number assay. PCR was performed on duplicate samples using the CFX96 Touch Real-Time PCR Detection System (BioRad).

### RNA sequencing data

Osteosarcoma RNA sequencing data was downloaded from the NCI TARGET Osteosarcoma database. B-acute lymphoblastic leukemia, T-acute lymphoblastic leukemia, mixed lineage leukemia, acute myeloid leukemia, low-grade glioma, ependymoma, high-grade glioma, medulloblastoma, choroid plexus carcinoma, rhabdomyosarcoma, melanoma, retinoblastoma, adrenocortical tumor, and osteosarcoma RNA sequencing data are part of the Pediatric Cancer Genome Project and was downloaded from the St. Jude Cloud PeCan Data Portal (<https://pecan.stjude.cloud/home>).<sup>69</sup>

### Immunohistochemistry

Osteosarcoma TMA slides were purchased from Novus Biologicals, the content of which are described in (Table 2). The TMAs were deparaffinized, rehydrated through graded ethanols, and subjected to heat induced epitope retrieval in citrate buffer pH 6 (Vector Laboratories). TMA slides were quenched of endogenous peroxidases, blocked in 2% normal horse serum, and incubated with anti-B7-H3 (14058 Cell Signaling) or anti-IDO1 (MAB5412; Millipore) antibodies overnight. Signal amplification was achieved using the VectaStain Elite ABC kit (Vector Laboratories). Color development was achieved with 3,3'-diaminobenzidine and counter stained with hematoxylin (Vector Laboratories). Immunoreactivity was scored by two board certified pediatric pathologists with extensive expertise in bone and soft tissue sarcomas (DWP and TJT). Cores were excluded from analysis if the patient age exceeded 40 years old, if the tissue was overly decalcified, if there was less than 25% of the core remaining on the slide, and/or if there was less than 25% tumor present in the core. Tissue cores were scored on the basis of percentage of positively stained tumor cells where a score of 0 = no tumor cells stained, 1 = up to 25% of tumor cells stained, 2 = 26–50% of tumor cells stained, 3 = 51–75% of tumor cells stained, and 4 = 76–100% of tumor cells stained. Tissue cores were also scored according to stain intensity where a score of 0 = negative/background, 1 = slightly above background, 2 = definitive light staining, 3 = medium staining, and 4 = intense staining. Both scores were multiplied to arrive at the final score that was used for downstream analysis. Images were captured using a Leica DMI6000B inverted microscope with a 10X objective. Positive controls and secondary antibody only controls are shown in Supplemental (Figure 2).

### Tryptophan assay

Conditioned media was collected after 24-hours of IFN $\gamma$  stimulation and cleared of cellular debris by centrifugation. Tryptophan levels in the conditioned media were assayed using the Bridge-It L-Tryptophan Fluorescence Assay (Mediomics) according to the manufacturers protocol.

### Western blotting

Cells were lysed in radioimmunoprecipitation buffer supplemented with protease/phosphatase inhibitors (ThermoFisher).

Protein concentrations were determined using the Pierce BCA assay (ThermoFisher). Samples were mixed with NuPAGE LDS sample buffer and Sample Reducing Agent (ThermoFisher), heated, separated on a Novex 4–12% Bis-Tris gradient gel (Thermo Fisher). Proteins were transferred to polyvinylidene fluoride membranes, blocked, and probed with antibodies against IDO1 (86630 Cell Signaling), B7-H3 (14058 Cell Signaling), or GAPDH-AlexaFlour 488 (#3906; Cell Signaling). Secondary anti-rabbit antibodies were purchased from Cell Signaling Technologies. Blots were sequentially probed with antibodies without stripping between primary antibody incubations. Chemiluminescent and fluorescent images were captured using the ChemiDoc MP imaging system (Bio-Rad).

### Statistical Analysis

All histograms, scatter plots, Kaplan-Meier curves, and associated statistical values were generated using Prism7 (GraphPad). P-values  $\leq 0.05$  are considered to be statistically significant. Correlation matrix was generated using Morpheus visualization and analysis software (<https://software.broadinstitute.org/morpheus/>). OncoPrints were generated using OncoPrinter ([www.cbioportal.org/oncoprinter.jsp](http://www.cbioportal.org/oncoprinter.jsp)).

### Financial Support

This work was supported by the National Cancer Institute under Grant 2P30CA014089-41 (TAM); a gift from the Colich family (TAM); and the Department of Defense under Grant W81XWH-07-1-0580 (TJT).

### Disclosure statement

No potential conflict of interest was reported by the authors.

### ORCID

Troy A McEachron  <http://orcid.org/0000-0003-0695-5783>

### References

- Chen X, Bahrami A, Pappo A, Easton J, Dalton J, Hedlund E, Ellison D, Shurtleff S, Wu G, Wei L, et al. Recurrent somatic structural variations contribute to tumorigenesis in pediatric osteosarcoma. *Cell Rep*. 2014. 7(1):104–112. doi:10.1016/j.celrep.2014.03.003.
- Kovac M, Blattmann C, Ribi S, Smida J, Mueller NS, Engert F, Castro-Giner F, Weischenfeldt J, Kovacova M, Krieg A, et al. Exome sequencing of osteosarcoma reveals mutation signatures reminiscent of BRCA deficiency. *Nat Commun*. 2015. 6:8940. doi:10.1038/ncomms9940.
- Lorenz S, Barøy T, Sun J, Nome T, Vodák D, Bryne JC, Håkelién AM, Fernandez-Cuesta L, Möhlendick B, Rieder H, et al. Unscrambling the genomic chaos of osteosarcoma reveals extensive transcript fusion, recurrent rearrangements and frequent novel TP53 aberrations. *Oncotarget*. 2016. 7(5):5273–5288. doi:10.18632/oncotarget.6567.
- Smida J, Xu H, Zhang Y, Baumhoer D, Ribi S, Kovac M, von Luetichau I, Bielack S, O'Leary VB, Leib-Mösch C, et al. Genome-wide analysis of somatic copy number alterations and chromosomal breakages in osteosarcoma. *Int J Cancer*. 2017. doi:10.1002/ijc.30778.
- Allison DC, Carney SC, Ahlmann ER, Hendifar A, Chawla S, Fedenko A, Angeles C, Menendez LR. A meta-analysis of osteosarcoma outcomes in the modern medical era. *Sarcoma*. 2012. 2012:704872. doi:10.1155/2012/704872.
- Reed DR, Hayashi M, Wagner L, Binitie O, Steppan DA, Brohl AS, Shinohara ET, Bridge JA, Loeb DM, Borinstein SC, et al. Treatment pathway of bone sarcoma in children, adolescents, and young adults. *Cancer*. 2017. doi:10.1002/cncr.30589.
- Adams JL, Smothers J, Srinivasan R, Hoos A. Big opportunities for small molecules in immuno-oncology. *Nat Rev Drug Discov*. 2015. 14(9):603–622. doi:10.1038/nrd4596.
- Fournier C, Martin F, Zitvogel L, Kroemer G, Galluzzi L, Trial Watch: AL. Adoptively transferred cells for anticancer immunotherapy. *OncoImmunology*. 2017. 6(11):e1363139. doi:10.1080/2162402X.2017.1363139.
- Rossi DL, Rossi EA, Cardillo TM, Goldenberg DM, Chang C-H. A new class of bispecific antibodies to redirect T cells for cancer immunotherapy. *mAbs*. 2014. 6(2):381–391. doi:10.4161/mabs.27385.
- Yuraszek T, Kasichayanula S, Benjamin J. Translation and clinical development of bispecific T-cell engaging antibodies for cancer treatment. *Clin Pharmacol Ther*. 2017. 101(5):634–645. doi:10.1002/cpt.651.
- Vacchelli E, Aranda F, Eggermont A, Sautès-Fridman C, Tartour E, Kennedy EP, Platten M, Zitvogel L, Kroemer G, Galluzzi L. Trial watch: IDO inhibitors in cancer therapy. *OncoImmunology*. 2014. 3(10):e957994. doi:10.4161/21624011.2014.957994.
- Hellmann MD, Rizvi NA, Goldman JW, Gettinger SN, Borghaei H, Brahmer JR, Ready NE, Gerber DE, Chow LQ, Juergens RA, et al. Nivolumab plus ipilimumab as first-line treatment for advanced non-small-cell lung cancer (CheckMate 012): results of an open-label, phase 1, multicohort study. *Lancet Oncol*. 2017. 18(1):31–41. doi:10.1016/S1470-2045(16)30624-6.
- Reck M, Rodríguez-Abreu D, Robinson AG, Hui R, Csósz T, Fülöp A, Gottfried M, Peled N, Tafreshi A, Cuffe S, et al. Pembrolizumab versus Chemotherapy for PD-L1-Positive Non-Small-Cell Lung Cancer. *N Engl J Med*. 2016. 375(19):1823–1833. doi:10.1056/NEJMoa1606774.
- Balar AV, Castellano D, O'Donnell PH, Grivas P, Vuky J, Powles T, Plimack ER, Hahn NM, de Wit R, Pang L, et al. First-line pembrolizumab in cisplatin-ineligible patients with locally advanced and unresectable or metastatic urothelial cancer (KEYNOTE-052): a multicentre, single-arm, phase 2 study. *Lancet Oncol*. 2017. Epub 2017/ 09/26. 18(11):1483–1492. doi:10.1016/S1470-2045(17)30616-2.
- Bellmunt J, de Wit R, Vaughn DJ, Fradet Y, Lee JL, Fong L, Vogelzang NJ, Climent MA, Petrylak DP, Choueiri TK, et al. Pembrolizumab as Second-Line Therapy for Advanced Urothelial Carcinoma. *N Engl J Med*. 2017. Epub 2017/ 02/17. 376(11):1015–1026. doi:10.1056/NEJMoa1613683.
- Herbst RS, Baas P, Kim DW, Felip E, Pérez-Gracia JL, Han JY, Molina J, Kim JH, Arvis CD, Ahn MJ, et al. Pembrolizumab versus docetaxel for previously treated, PD-L1-positive, advanced non-small-cell lung cancer (KEYNOTE-010): a randomized controlled trial. *Lancet*. 2016. Epub 2015/ 12/30. 387(10027):1540–1550. doi:10.1016/s0140-6736(15)01281-7.
- US Food and Drug Administration. Hematology/Oncology (Cancer) Approvals & Safety Notifications 2018 [Accessed March 7, 2018]. Available from: <https://www.fda.gov/Drugs/InformationOnDrugs/ApprovedDrugs/ucm279174.htm>.
- D'Angelo SP, Mahoney MR, Van Tine BA, Atkins J, Milhem MM, Jahagirdar BN, Antonescu CR, Horvath E, Tap WD, Schwartz GK, et al. Nivolumab with or without ipilimumab treatment for metastatic sarcoma (Alliance A091401): two open-label, non-comparative, randomized, phase 2 trials. *Lancet Oncol*. 2018. 19(3):416–426. doi:10.1016/S1470-2045(18)30006-8.
- Merchant MS, Wright M, Baird K, Wexler LH, Rodriguez-Galindo C, Bernstein D, Delbrook C, Lodish M, Bishop R, Wolchok JD, et al. Phase I Clinical Trial of Ipilimumab in Pediatric Patients with Advanced Solid Tumors. *Clin Cancer Res*. 2016. 22(6):1364–1370. doi:10.1158/1078-0432.CCR-15-0491.

20. Tawbi HA, Burgess M, Bolejack V, Van Tine BA, Schuetze SM, Hu J, D'Angelo S, Attia S, Riedel RF, Priebat DA, et al. Pembrolizumab in advanced soft-tissue sarcoma and bone sarcoma (SARC028): a multicentre, two-cohort, single-arm, open-label, phase 2 trial. *Lancet Oncol*. 2017. 18(11):1493–1501. doi:10.1016/S1470-2045(17)30624-1.
21. Tawbi HA-H, Burgess MA, Crowley J, Van Tine BA, Hu J, Schuetze S, D'Angelo SP, Attia S, Priebat DA, Okuno SH, et al. Safety and efficacy of PD-1 blockade using pembrolizumab in patients with advanced soft tissue (STS) and bone sarcomas (BS): results of SARC028—A multicenter phase II study. *J Clin Oncol*. 2016. 34(15\_suppl):11006. doi:10.1200/JCO.2016.34.15\_suppl.11006.
22. Schultz LM, Majzner R, Davis KL, Mackall C. New developments in immunotherapy for pediatric solid tumors. *Curr Opin Pediatr*. 2017. 1. doi:10.1097/MOP.0000000000000564.
23. Davoli T, Uno H, Wooten EC, Elledge SJ. Tumor aneuploidy correlates with markers of immune evasion and with reduced response to immunotherapy. *Science (New York, NY)*. 2017. 355:6322. doi:10.1126/science.aaf8399.
24. Shen JK, Cote GM, Choy E, Yang P, Harmon D, Schwab J, Nielsen GP, Chebib I, Ferrone S, Wang X, et al. Programmed Cell Death Ligand 1 Expression in Osteosarcoma. *Cancer Immunol Res*. 2014. 2(7):690–698. doi:10.1158/2326-6066.CIR-13-0224.
25. Koirala P, Roth ME, Gill J, Piperdi S, Chinai JM, Geller DS, Hoang BH, Park A, Fremed MA, Zang X, et al. Immune infiltration and PD-L1 expression in the tumor microenvironment are prognostic in osteosarcoma. *Sci Rep*. 2016. 6:1. doi:10.1038/srep30093.
26. Zheng B, Ren T, Huang Y, Sun K, Wang S, Bao X, Liu K, Guo W. PD-1 axis expression in musculoskeletal tumors and antitumor effect of nivolumab in osteosarcoma model of humanized mouse. *J Hematol Oncol*. 2018. 11:1. doi:10.1186/s13045-018-0560-1.
27. Lussier DM, Johnson JL, Hingorani P, Blattman JN. Combination immunotherapy with  $\alpha$ -CTLA-4 and  $\alpha$ -PD-L1 antibody blockade prevents immune escape and leads to complete control of metastatic osteosarcoma. *J for ImmunoTherapy of Cancer*. 2015. 3:1. doi:10.1186/s40425-015-0067-z.
28. Lussier DM, O'Neill L, Nieves LM, McAfee MS, Holechek SA, Collins AW, Dickman P, Jacobsen J, Hingorani P, Blattman JN. Enhanced T-cell immunity to osteosarcoma through antibody blockade of PD-1/PD-L1 interactions. *J Immunotherapy (Hagerstown, Md: 1997)*. 2015. 38(3):96–106. doi:10.1097/CJI.0000000000000065.
29. Prendergast GC, Mondal A, Dey S, Laury-Kleintop LD, Muller AJ. Inflammatory Reprogramming with IDO1 Inhibitors: turning Immunologically Unresponsive 'Cold' Tumors 'Hot'. *Trends in Cancer*. 2018. 4(1):38–58. doi:10.1016/j.trecan.2017.11.005.
30. Van Baren N, Van den Eynde BJ. Tumoral Immune Resistance Mediated by Enzymes That Degrade Tryptophan. *Cancer Immunol Res*. 2015. 3(9):978–985. doi:10.1158/2326-6066.CIR-15-0095.
31. Barrett MT, Anderson KS, Lenkiewicz E, Andreozzi M, Cunliffe HE, Klassen CL, Dueck AC, McCullough AE, Reddy SK, Ramanathan RK, et al. Genomic amplification of 9p24.1 targeting *JAK2*, *PD-L1*, and *PD-L2* is enriched in high-risk triple negative breast cancer. *Oncotarget*. 2015. 6(28): doi:10.18632/oncotarget.4494.
32. Inoue Y, Yoshimura K, Mori K, Kurabe N, Kahyo T, Mori H, Kawase A, Tanahashi M, Ogawa H, Inui N, et al. Clinical significance of *PD-L1* and *PD-L2* copy number gains in non-small-cell lung cancer. *Oncotarget*. 2016. 7:22. doi:10.18632/oncotarget.8528.
33. George J, Saito M, Tsuta K, Iwakawa R, Shiraiishi K, Scheel AH, Uchida S, Watanabe SI, Nishikawa R, Noguchi M, et al. Genomic Amplification of *CD274* (PD-L1) in Small-Cell Lung Cancer. *Clin Cancer Res*. 2017. 23(5):1220–1226. doi:10.1158/1078-0432.CCR-16-1069.
34. Loo D, Alderson RF, Chen FZ, Huang L, Zhang W, Gorlatov S, Burke S, Ciccarone V, Li H, Yang Y, et al. Development of an Fc-Enhanced Anti-B7-H3 monoclonal antibody with potent antitumor activity. *Clin Cancer Res*. 2012. 18(14):3834–3845. doi:10.1158/1078-0432.CCR-12-0715.
35. Seaman S, Zhu Z, Saha S, Zhang XM, Yang MY, Hilton MB, Morris K, Szot C, Morris H, Swing DA, et al. Eradication of tumors through simultaneous ablation of CD276/B7-H3-positive tumor cells and tumor vasculature. *Cancer Cell*. 2017. 31(4):501–15.e8. doi:10.1016/j.ccell.2017.03.005.
36. Al-Sukaini A, Hornicek FJ, Peacock ZS, Kaban LB, Ferrone S, Schwab JH. Immune surveillance plays a role in locally aggressive giant cell lesions of bone. *Clin Orthopaedics Relat Research*. 2017. 475(12):3071–3081. doi:10.1007/s11999-017-5451-1.
37. Kraan J, Van Den Broek P, Verhoef C, Grunhagen DJ, Taal W, Gratama JW, Sleijfer S. Endothelial CD276 (B7-H3) expression is increased in human malignancies and distinguishes between normal and tumour-derived circulating endothelial cells. *Br J Cancer*. 2014. 111(1):149–156. doi:10.1038/bjc.2014.286.
38. Suh WK, Wang SX, Jheon AH, Moreno L, Yoshinaga SK, Ganss B, Sodek J, Grynaps MD, Mak TW. The immune regulatory protein B7-H3 promotes osteoblast differentiation and bone mineralization. *Proc Natl Acad Sci*. 2004. 101(35):12969–12973. doi:10.1073/pnas.0405259101.
39. Xu L, Zhang G, Zhou Y, Chen Y, Xu W, Wu S, Zhang X. Stimulation of B7-H3 (CD276) directs the differentiation of human marrow stromal cells to osteoblasts. *Immunobiology*. 2011. 216(12): 1311–1317. doi:10.1016/j.imbio.2011.05.013.
40. Chapoval AI, Ni J, Lau JS, Wilcox RA, Flies DB, Liu D, Dong H, Sica GL, Zhu G, Tamada K, et al. B7-H3: a costimulatory molecule for T cell activation and IFN-gamma production. *Nat Immunol*. 2001. 2(3):269–274. doi:10.1038/85339.
41. Li G, Quan Y, Che F, Wang L. B7-H3 in tumors: friend or foe for tumor immunity? *Cancer Chemother Pharmacol*. Epub 2018/ 01/ 03. 2018. 81(2):245–253. doi:10.1007/s00280-017-3508-1.
42. Suh WK, Gajewska BU, Okada H, Gronski MA, Bertram EM, Dawicki W, Duncan GS, Buczynski J, Plyte S, Elia A, et al. The B7 family member B7-H3 preferentially down-regulates T helper type 1-mediated immune responses. *Nat Immunol*. Epub 2003/ 08/17. 2003. 4(9):899–906. doi:10.1038/ni967.
43. Yonesaka K, Haratani K, Takamura S, Sakai H, Kato R, Takegawa N, Takahama T, Tanaka K, Hayashi H, Takeda M, et al. B7-H3 negatively modulates CTL-mediated cancer immunity. *Clin Cancer Res*. Epub 2018/ 03/12. 2018. doi:10.1158/1078-0432.CCR-17-2852.
44. Mao L, Fan TF, Wu L, Yu GT, Deng WW, Chen L, Bu LL, Ma SR, Liu B, Bian Y, et al. Selective blockade of B7-H3 enhances antitumor immune activity by reducing immature myeloid cells in head and neck squamous cell carcinoma. *J Cell Mol Med*. Epub 2017/ 04/11. 2017. 21(9):2199–2210. doi:10.1111/jcmm.13143.
45. Wang L, Zhang Q, Chen W, Shan B, Ding Y, Zhang G, Cao N, Liu L, Zhang Y. B7-H3 is overexpressed in patients suffering osteosarcoma and associated with tumor aggressiveness and metastasis. *PLoS ONE*. 2013. 8(8):e70689. doi:10.1371/journal.pone.0070689.
46. Picarda E, Ohaegbulam KC, Molecular Pathways: ZX. Targeting B7-H3 (CD276) for human cancer immunotherapy. *Clin Cancer Res*. 2016. 22(14):3425–3431. doi:10.1158/1078-0432.CCR-15-2428.
47. Walker AJ, Majzner RG, Zhang L, Wanhainen K, Long AH, Nguyen SM, Lopomo P, Vigny M, Fry TJ, Orentas RJ, et al. Tumor antigen and receptor densities regulate efficacy of a chimeric antigen receptor targeting anaplastic lymphoma kinase. *Mol Ther*. Epub 2017/ 07/01. 2017. 25(9):2189–2201. doi:10.1016/j.ymthe.2017.06.008.
48. Litzenger UM, Opitz CA, Sahm F, Rauschenbach KJ, Trump S, Winter M, Ott M, Ochs K, Lutz C, Liu X, et al. Constitutive IDO expression in human cancer is sustained by an autocrine signaling loop involving IL-6, STAT3 and the AHR. *Oncotarget*. 2014. 5(4):1038–1051. doi:10.18632/oncotarget.1637.
49. Liebau C, Baltzer AWA, Schmidt S, Roesel C, Karreman C, Prisack JB, Bojar H, Merk H. Interleukin-12 and interleukin-18

- induce indoleamine 2,3-dioxygenase (IDO) activity in human osteosarcoma cell lines independently from interferon-gamma. *Anticancer Res.* 2002. 22(2A):931–936.
50. Flores RJ, Kelly AJ, Li Y, Nakka M, Barkauskas DA, Krailo M, Wang LL, Perlaky L, Lau CC, Hicks MJ, et al. A novel prognostic model for osteosarcoma using circulating CXCL10 and FLT3LG. *Cancer.* 2017. 123(1):144–154. doi:10.1002/cncr.30272.
  51. Urakawa H, Nishida Y, Nakashima H, Shimoyama Y, Nakamura S, Ishiguro N. Prognostic value of indoleamine 2,3-dioxygenase expression in high grade osteosarcoma. *Clin Exp Metastasis.* 2009. 26(8):1005–1012. doi:10.1007/s10585-009-9290-7.
  52. Taylor NP. Bristol-Myers Squibb drops phase 3 trials of \$800M IDO drug: Fierce Biotech; 2018 [Accessed 05 March 2018]. Available from: <https://www.fiercebiotech.com/biotech/bristol-myers-drops-phase-3-trials-800m-ido-drug>.
  53. Taylor NP. Incyte wipes out late-phase epacadostat program after pivotal failure of Keytruda combination Fierce Biotech 2018 [Accessed 05 March 2018]. Available from: <https://www.fiercebiotech.com/biotech/incyte-wipes-out-late-phase-epacadostat-program-after-pivotal-failure-keytruda-combination>.
  54. Zhao Q, Kuang D-M, Wu Y, Xiao X, Li X-F, Li T-J, Zheng L. Activated CD69+ T cells foster immune privilege by regulating IDO expression in tumor-associated macrophages. *Journal of Immunology (Baltimore, Md: 1950).* 2012. 188(3):1117–1124. doi:10.4049/jimmunol.1100164.
  55. Li T, Yang Y, Hua X, Wang G, Liu W, Jia C, Tai Y, Zhang Q, Chen G. Hepatocellular carcinoma-associated fibroblasts trigger NK cell dysfunction via PGE2 and IDO. *Cancer Lett.* 2012. 318(2):154–161. doi:10.1016/j.canlet.2011.12.020.
  56. Riesenberger R, Weiler C, Spring O, Eder M, Buchner A, Popp T, Castro M, Kammerer R, Takikawa O, Hatz RA, et al. Expression of indoleamine 2,3-dioxygenase in tumor endothelial cells correlates with long-term survival of patients with renal cell carcinoma. *Clin Cancer Res.* 2007. 13(23):6993–7002. doi:10.1158/1078-0432.CCR-07-0942.
  57. Chen J-Y, Li C-F, Kuo C-C, Tsai K-K, Hou M-F, Hung W-C. Cancer/stroma interplay via cyclooxygenase-2 and indoleamine 2,3-dioxygenase promotes breast cancer progression. *Breast Cancer Res.* 2014. 16:4. doi:10.1186/s13058-014-0410-1.
  58. Théate I, van Baren N, Pilotte L, Moulin P, Larrieu P, Renaud JC, Hervé C, Gutierrez-Roelens I, Marbaix E, Sempoux C, et al. Extensive profiling of the expression of the indoleamine 2,3-dioxygenase 1 protein in normal and tumoral human tissues. *Cancer Immunol Res.* 2015. 3(2):161–172. doi:10.1158/2326-6066.CIR-14-0137.
  59. Shibata Y, Hara T, Nagano J, Nakamura N, Ohno T, Ninomiya S, Ito H, Tanaka T, Saito K, Seishima M, et al. The role of indoleamine 2,3-dioxygenase in diethylnitrosamine-induced liver carcinogenesis. *PLoS One.* 2016. 11(1):e0146279. doi:10.1371/journal.pone.0146279.
  60. Holmgaard RB, Zamarin D, Li Y, Gasmi B, Munn DH, Allison JP, Merghoub T, Wolchok JD. Tumor-expressed IDO recruits and activates MDSCs in a Treg-dependent manner. *Cell Rep.* 2015. 13(2):412–424. doi:10.1016/j.celrep.2015.08.077.
  61. Giesen C, Wang HA, Schapiro D, Zivanovic N, Jacobs A, Hattendorf B, Schüffler PJ, Grolimund D, Buhmann JM, Brandt S, et al. Highly multiplexed imaging of tumor tissues with sub-cellular resolution by mass cytometry. *Nature Methods.* 2014. 11(4):417–422. doi:10.1038/nmeth.2869.
  62. Schelker M, Feau S, Du J, Ranu N, Klipp E, MacBeath G, Schoeberl B, Raue A. Estimation of immune cell content in tumour tissue using single-cell RNA-seq data. *Nat Commun.* 2017. 8:1. doi:10.1038/s41467-017-02289-3.
  63. Prendergast GC, Smith C, Thomas S, Mandik-Nayak L, Laury-Kleintop L, Metz R, Muller AJ. Indoleamine 2,3-dioxygenase pathways of pathogenic inflammation and immune escape in cancer. *Cancer Immunology, Immunotherapy: CII.* 2014. 63(7):721–735. doi:10.1007/s00262-014-1549-4.
  64. Paoluzzi L, Cacavio A, Ghesani M, Karambelkar A, Rapkiewicz A, Weber J, Rosen G. Response to anti-PD1 therapy with nivolumab in metastatic sarcomas. *Clin Sarcoma Res.* 2016. 6:1. doi:10.1186/s13569-016-0064-0.
  65. Groisberg R, Hong DS, Behrang A, Hess K, Janku F, Piha-Paul S, Naing A, Fu S, Benjamin R, Patel S, et al. Characteristics and outcomes of patients with advanced sarcoma enrolled in early phase immunotherapy trials. *J for ImmunoTherapy of Cancer.* 2017. 5:1. doi:10.1186/s40425-017-0301-y.
  66. Toulmonde M, Penel N, Adam J, Chevreau C, Blay JY, Le Cesne A, Bompas E, Piperno-Neumann S, Cousin S, Grellety T, et al. Use of PD-1 targeting, macrophage infiltration, and IDO pathway activation in sarcomas: a phase 2 clinical trial. *JAMA Oncology.* 2018. 4(1):93. doi:10.1001/jamaoncol.2017.1617.
  67. Holmgaard RB, Zamarin D, Munn DH, Wolchok JD, Allison JP. Indoleamine 2,3-dioxygenase is a critical resistance mechanism in antitumor T cell immunotherapy targeting CTLA-4. *J Exp Med.* 2013. 210(7):1389–1402. doi:10.1084/jem.20130066.
  68. Dix Junqueira Pinto G, De Souza Viana L, Scapulatempo NC, Vicente SS. Evaluation of PD-L1 expression in tumor tissue of patients with lung carcinoma and correlation with clinical and demographic data. *J Immunol Res.* 2016. Epub 2016/ 09/22. 2016: 9839685. doi:10.1155/2016/9839685.
  69. Downing JR, Wilson RK, Zhang J, Mardis ER, Pui CH, Ding L, Ley TJ, Evans WE. The pediatric cancer genome project. *Nat Genet.* 2012. Epub 2012/ 05/29. 44(6):619–622. doi:10.1038/ng.2287.